Answers to Anonymous Referee #1

We thank the anonymous referee #1 for his/her constructive comments and suggestions that certainly have improved the manuscript significantly. We revised the manuscript according to his/her comments and the comments of anonymous referees #2 and #3. In the following,

- *referee's comments are given in italic*,
- our answers are outlined in normal format, and
- **textual changes in the manuscript are given in bold format**.

We would like inform the anonymous referee #1 about the following changes:

1. Driven by the specific comment (SC) #18 of anonymous referee #3 (SC3.18), we decided to drop scenario S4 from the analysis. The difference between the sub-adiabatic model (S3) and the modified one (S4) is that the latter accounts for the depletion of the liquid water content due to entrainment, precipitation, and freezing drops. Consequently, we wanted to check whether S4 captures better the vertical stratification of the modeled low-level clouds and, accordingly, if it approximates the CREs of the reference simulation with better accuracy. Since S4 does not provide any further insight, we now have decided to drop this scenario. However, we do confirm that, by considering all the case days in the analysis, we came to the same conclusions as for 3 June. As a confirmation, we updated the Tables and attached them at the end of this document. The referee is referred to Tables R1–R3.

2. In all scenarios, we decided to drop sub-case d, which employs two fixed values for the droplet number concentration representing the two modes in the corresponding histogram for 3 June 2016. This scenario separates clouds into a cluster with low/high clouds. Considering the vertical variability of the droplet number concentration, the latter clustering will link low clouds (within the boundary layer) with high N_d and, accordingly, high clouds with lower N_d values. Thus, for all scenarios, employing such values for N_d are able to approximate the reference radiative transfer simulation very well. Only the radiative transfer simulation that is supplied by the droplet number concentration weighted over the cloud geometrical extent, i.e., N_int (sub-case b) leads to smaller differences when compared to the reference simulation. However, we do confirm that, by considering all the case days into the analysis, we came to the same conclusions as for 3 June. Note that, for the latter case, the clustering was conducted on the mean N_int over all case days. As a confirmation, we updated the Tables and attached them at the end of this document. The referee is referred to Tables R1–R3.

3. We decided to add a new scenario as a replacement of sub-case d, whereby radiative transfer simulations are conducted for a mean vertical profile of the droplet number concentration over all case days. Tables R9–R11 summarize the new results. In brief, this scenario is considered as an improvement compared to the clustering case. The following parts were included within the text:

   Section 5.1.2: **Last but not least, by replacing the vertical profile of N_d by the**

mean profile of N_d over all case days (see Fig. 2), emulates the cloud radiative effects of the reference simulation quite well. Accordingly, scenario S4 slightly undersimates the mean SW CREs, with an mean error up to $-3.16\,\mathrm{W\,m^{-2}}$ and a RMSE up to $17.2\,\mathrm{W\,m^{-2}}$ for both BOA and TOA. In fact, this scenario outperforms the rest scenarios (S1–S3), except from the sub-case b (N_{int}) in all scenarios. For an illustration of the excellent linear correlation between the reference simulation and S4 by means of a bivariate kernel density (BKD) plot, the reader is referred to Fig. B1 in Appendix B. One can see that the CREs computed by these scenarios are in a very good agreement almost everywhere except towards larger values of the CREs in case of the SW radiation, with Pearson correlations larger than 0.977 for both BOA and TOA.

Section 6: **By employing a more representative profile for the N_d, i.e., a mean vertical profile of N_d over all case days leads to a rather good approximation; the RMSE is below $17.2\,\mathrm{W\,m^{-2}}$. This points to the need to better account for prognostic N_d calculations.**

Appendix B: **In sect. 5.1.2, by conducting idealized radiative transfer simulations, we estimated the impact of the representation of cloud properties in ICON-LEM on the cloud radiative effects (CREs). Special emphasis was given on identifying the droplet number concentration (N_d), which approximates the microphysical and radiative properties of low-level clouds as simulated by ICON-LEM (reference scenario). A radiative transfer simulation, which employs a mean vertical profile of N_d over all the case days (scenario S4), approximates the CREs of the reference scenario quite well. Figure B1 depicts the excellent linear correlation between the reference simulation and S4 by means of a bivariate kernel density (BKD)**.

4. Following the general comment of anonymous referee #2 for shortening the manuscript given the redundancy of many of the results shown in this study and his/her relevant specific comments (SC), i.e., (SC2.12) and (SC2.25):

   - We decided to drop Fig. B1. Figure B1 illustrates the bivariate kernel density (BKD) between the cloud optical thickness and the liquid water path on a logarithmic scale. Considering the comprehensive explanation given in Sect. 3.3.1, we decided that this illustration did not provide any additional information.
   - Figures 6 and 7 have been revised. Now, they illustrate results only for TOA (see Figs R2 and R3).
   - We now focus only on the rotational component analysis. The mention of the principal component analysis have been significantly reduced. In addition, we removed the relevant information from Table 3. For the updated version of the Table, the referees are referred to Table R5. Additionally, we replaced Figure 5 by Table R4. This table lists the contribution of each rotational component to the total variance.

Answers to general comments (GC) from referee #1 (GC1)

(GC1.1) *My major concern is that the simulations examined in this study are very limited (Page 8 Line 15-18). The authors conducted simulations using six case days, but actually looked at in details only the case of 3 June 2016. How general are they? Doesn't the vertical structure of adiabaticity depend strongly on the cloud regimes and types or their life-stage? In the present form of this paper, objectives are too narrow. The described relationship among cloud micro- and macrophysical properties and radiative effect using high resolution simulation may provide key suggestions on aerosol-cloud interactions, but the findings as they are, are by no means general. With some more simulation cases or a bit more analysis for all the case days in detail, I think this will make a publishable work.*

These days have been selected from the total set of available case days by the presence of suitable liquid water cloud fields and no known bugs in the used model version, which affect the representation of low-level clouds. We do agree that the vertical structure of adiabaticity depends on cloud regimes, types, and life-stage and, thus, it could be an interesting extension. However, due to the high horizontal resolution of ICON-LEM, for a single day, the number of "independent" cloudy columns are very large and complicates the investigation of such dependencies. Note here that the model output employed in this study, 3D HOPE data, has an output frequency of 15 min, while the domain size is limited to 45 km^2. For such studies, especially when it comes to life-stage, it would be better to use model data with higher output frequency, e.g., 1D profiles that are available every 10 sec. But, this is beyond the purpose of this study. However, we revised our manuscript according to the comments of anonymous referee #1 and the comments of anonymous referees #3 further extended our analysis over all days to improve the robustness of our results. Now, sections 3.2 and 5 outline our findings for all case days.

As we aforementioned, throughout this study, a special emphasis was given to 3 June 2016, because, regardless of the large variability in cloud properties for each day, it approximates best the mean properties over all the case days considered. Thus, the revision of these two plots did not require any significant textual alteration (see Fig. R1 and Fig. R2); only minor textual changes were made.

Answers to specific comments (SC) from referee #1 (SC1)

(SC1.1) *Section 2.3: Please describe the model resolution, domain size, as well as timestep used in the simulations. The general description of ICON-LEM on page 3 (L16-17 and L28-30) is confusing with regards to this.*

We revised the description of ICON-LEM (Section 2.1) according to this comment and the specific comment (SC) # 3 of anonymous referee #3 (SC3.3):

The ICON unified modeling framework was co-developed by the German meteorological service (DWD) and the Max Planck institute for meteorology (MPI-M) in order to support climate research and weather forecasting. Within the HD(CP)2 project, ICON was further extended towards large eddy simulations with realistic topography **and** open boundary conditions. This resulted in

ICON-LEM **deployed in restricted areas that are centered on Germany and the Tropical Atlantic [1]. The equations utilized by the model are based on the prognostic variables given by Gassmann and Herzog [2]. These variables comprise the horizontal and vertical velocity components, the density of moist air, the virtual potential temperature, and the mass and number densities of traces, e.g., specific humidity, liquid water, and different ice hydrometeors. A comprehensive description of the model and its governing equations is found in Dipankar et al. [3] and Wan et al., [4].** Concerning turbulence parameterization, the three-dimensional Smagorinsky scheme is employed [3]. The activation of cloud condensation nuclei (CCN) is based on the parameterization of Seifert and Beheng [5] and modified in order to account for the consumption of CCNs due to their activation into cloud droplets. The CCN concentration is then parameterized following the pressure profile and the vertical velocity [6].

Simulations are carried out for three different domains with 624 m, 312 m, and 156 m horizontal resolution. The model domains consist of 150 vertical levels, with resolutions ranging from ∼25 m to 70 m within the boundary layer, and from 70 m to 355 m further up until the top of the domain at 21 km. For each of the aforementioned grids, data is stored as one-dimensional (1D) profiles every 10 sec, two-(2D), and 3D snapshots [1]. The model yields output on each of the aforementioned grids with the data stored as one-dimensional (1D) profiles, two-(2D), and 3D snapshots [1]. In case of the 3D output, the simulation data is interpolated from the original grids (e.g., 156 m) to a 1 km grid, the 3D coarse data, and 300 m grid, the so-called HOPE data. The latter output has been created for the purpose of model evaluation with ground-based observations from the HD(CP)^2 Observational Prototype Experiment (HOPE) that took place near Jülich [7]**and is limited to a domain size of about ∼45 km^2. Note here that for the 2D and 3D output, data is stored at day- and night-time frequency. Day-time frequency begins at 06:00 UTC and lasts until 00:00 UTC, while night-time starts at midnight and lasts until 06:00 UTC. The 2D data is stored with a day-time and night-time frequency of 10 sec and 5 min, respectively. The 3D coarse data have day-time frequency of 10 min (1 hour at night-time). In this study, the 3D HOPE data has been used that is stored only at a day-time frequency of 15 min.**

(SC1.2) *Equation (7): It is better to add a sentence about the factor* 2/3*, rather than* 5/9*, citing relevant papers (e.g., Szczodrak et al., 2001; Wood and Hartmann, 2006; Lebsock and Su, 2014). Equations (14) and (15) as well.*

We revised section 2.6 according to this comment and the specific comment (SC) #4 of anonymous referee #3 (SC3.4). The following parts have been added:

P6 L24: **while the factor** 2/3 **is a scale factor resulting from the constant liquid water content and effective radius with height [8].**

P7 L21: **Compared to Eq. (7), Eq. (10) leads to a factor of** 5/9**, meaning that the sub-adiabatic liquid water path is** 5/6 **times the one of the vertically homogeneous model [9].**

P8 L11: **For vertically constant q_{L} and r_{eff}, this can be interpreted as the cloud optical thickness coming from the vertical homogeneous model (see Eq. 7). According**

to the sub-adiabatic cloud model, the cloud optical thickness is linked to the liquid water path and the effective radius [10],

$$\tau = \frac{9}{5}\frac{Q_{\mathrm{L}}}{\rho_{\mathrm{w}} \cdot r_{\mathrm{eff}}}$$

Alternatively, substituting r_{eff} from Eq. (13) in Eq. (15), the cloud optical thickness is given by,...

(SC1.3) *Figure 3 and caption: q_{L} -¿ Q_{L} or CLWP.*

Actually, Fig. 3 illustrates the mean liquid water content profile normalized over the cloud geometrical extent. Throughout the paper, liquid water content is denoted as q_{L}.

(SC1.4) *Figures 6, 7 and 8: The order of sub-figures is not consistent with the caption.*

The order of sub-figures has been revised for consistency.

(SC1.5) *Table 6: I found several mismatches between Table 6 and citing main text (e.g., P18 L16), which made reviewers very difficult to track...*

We apologize for the mismatches. We have now extended the analysis to all case days and, thus, tables and related text have been revised.

(SC1.6) *P23 L11-13: This sentence is too vague. Please raise more specific source of uncertainty, and describe how the scrutinization is required.*

After the additional insight given by anonymous referee #2 (see general comment 3, i.e., GC2.3) we have revised this part of the text as follows:

The vertical variability of the droplet number concentration was examined. **For all the case days**, above an altitude of **about** 2 km, values of N_{d} are about 200 cm^{-3} and are, thus, close to climatological values, while in the boundary layer, the double moment scheme predicts N_{d} values above 600 cm^{-3}. Such values are **regarded as** rather high compared to satellite remote sensing estimates [11, 12], **but such comparison is rather vague considering, firstly, the large uncertainties of the satellite-derived estimates of cloud droplet number concentration [12] and, secondly, they are not available in high resolution. However,** in situ observations, **which are considered to be the most accurate approach to determine N_{d},** suggest higher values and, hence, lie closer to those simulated by ICON-LEM. **Thus, by means of in situ observations, evaluation activities should be conducted for a better characterization of the droplet number concentration from remote sensing techniques. The latter will scrutinize the double-moment scheme implemented in ICON-LEM and could potentially lead to better simulations of cloud processes and radiation.**

We additionally revised the corresponding text in Section 3.2 as follows,

On the contrary, in situ observations suggest higher values of N_{d} and, accordingly, closer to those simulated by ICON-LEM. **Hence, efforts should be undertaken to further validate**

the cloud droplet number concentrations predicted by the double-moment scheme.

(SC1.7) *P25 L12-L13: This sentence recommends double-moment cloud microphysics, but P23 L12 points weakness of the double-moment.*

After the insight given by the anonymous referee #2, the sentence at page 23, line 12, has been revised (see SC.6).

(SC1.8) *Appendix B: Please change the appendix title. Appendix section is not just a list of supporting materials. The current version does not have any explanation about the figures in the appendix (Appendix C as well).*

The Appendix B and C have been revised.

List of Figures

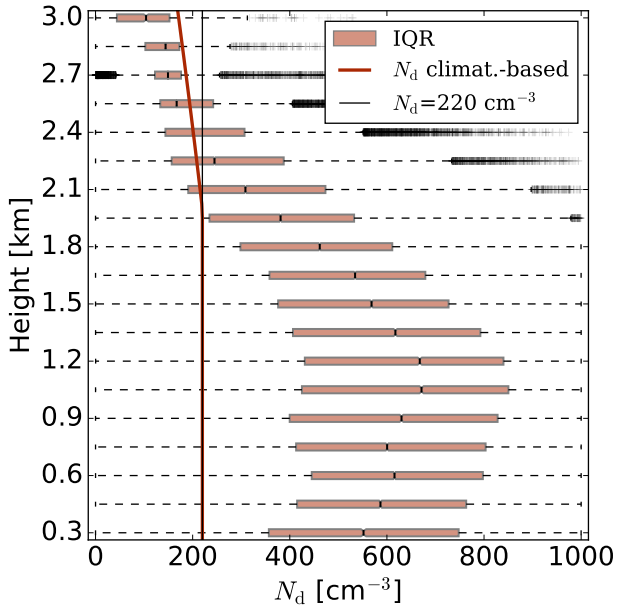

Figure R1: Box-whisker plot of the droplet number concentration for all the case days on average, describing the histograms of N_d simulated for different model levels by the double moment scheme of ICON-LEM. Boxes illustrate interquartile range (IQR), dark red line denotes the vertical N_d profile in case of the droplet number concentration employed in coarse climate models (climat.-based) and the thin black line demonstrates the constant N_d profile of 220 cm^{-3}.

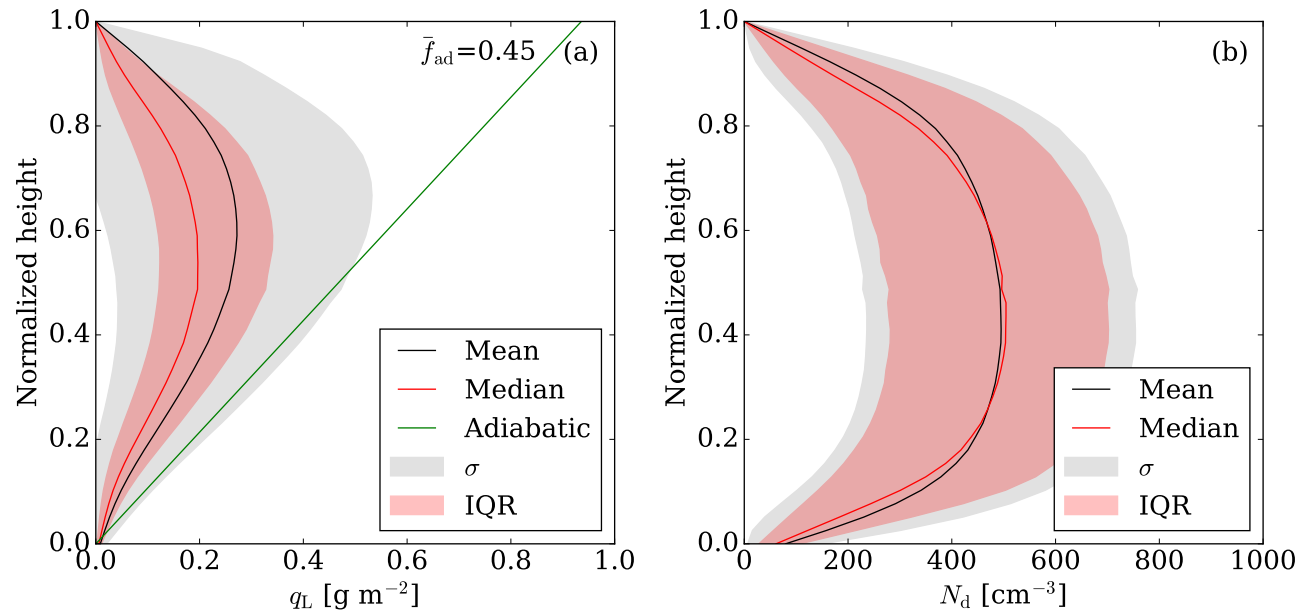

Figure R2: ICON-LEM simulated mean (a) q_L and (b) N_d profiles for all the case days on average. Profiles are normalized over height from the CBH to the CTH. Black lines denote the mean, red solid lines the median, gray shaded areas the standard deviation, red shaded areas the interquartile range (IQR), and the green solid line outline the mean adiabatic q_L profile characterized by a mean adiabatic fraction ($\bar{f}_{ad}$) of 0.45.

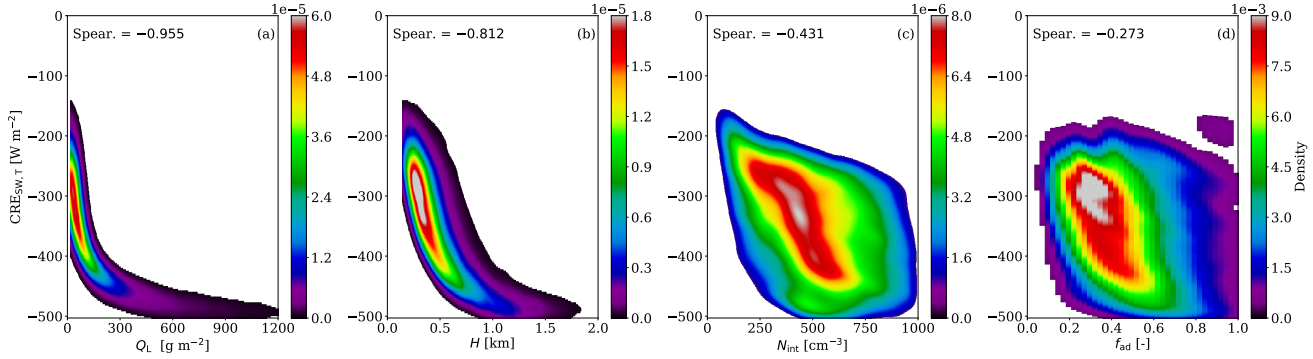

Figure R3: Bivariate kernel density (BKD) between the reference simulation (Ref.) and the cloud properties that are essential for the derivation of the cloud optical thickness that is one of the fundamental properties describing the SW cloud radiative effect. Panels illustrate the BKD between the $CRE_{SW,T}$ and (a) Q_L, (b) H, (c) N_{int}, and (d) f_{ad}. The corresponding Spearman (Spear.) correlations are highlighted.

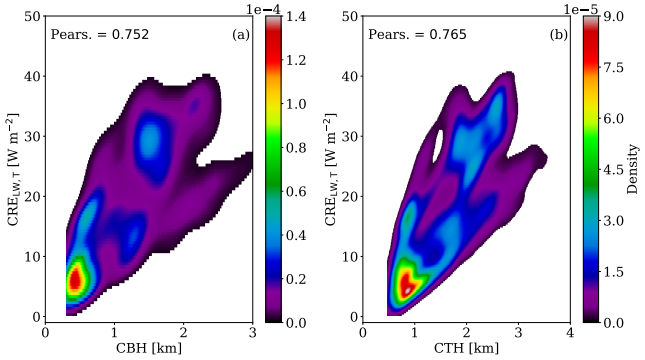

Figure R4: Bivariate kernel density (BKD) between the reference simulation (Ref.) and the cloud properties describing the LW cloud radiative effect at the BOA and (a) CBH and (b) CTH. The corresponding Pearson (Pears.) correlations are highlighted.

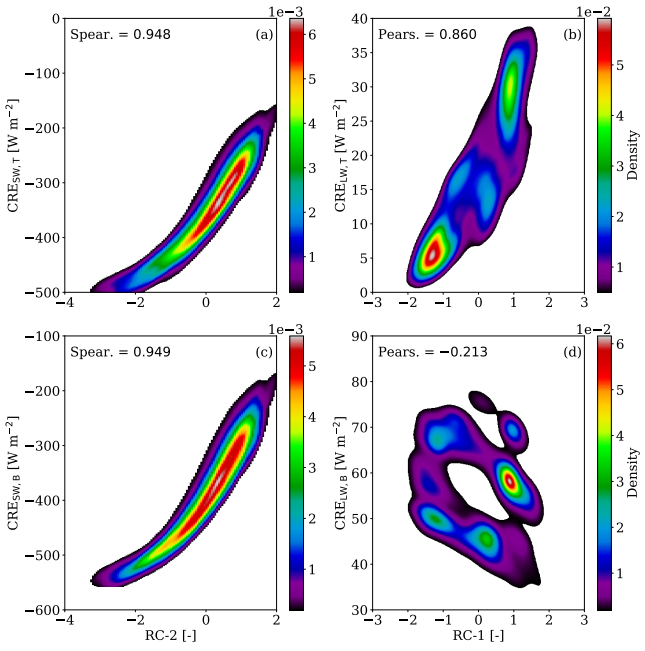

Figure R5: For the reference simulation (Ref.), bivariate kernel density (BKD) between CRE_{SW} and the second rotational component (RC-2) at (a) TOA, (c) BOA and between CRE_{LW} and the first rotational component (RC-1) at (b) TOA, (d) BOA. The corresponding Spearman (Spear.) and Pearson (Pears.) correlations are highlighted for the SW and LW radiation, respectively.

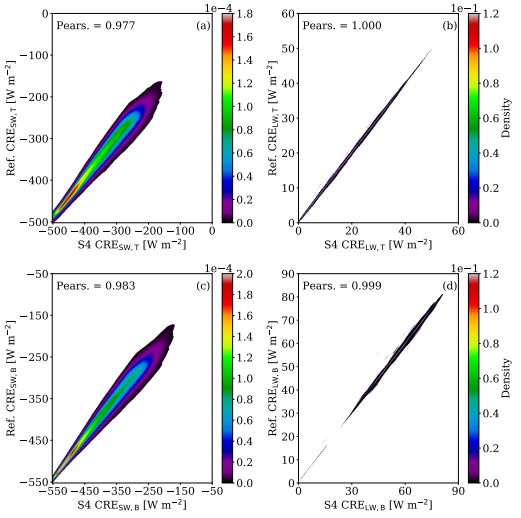

Figure R6: Bivariate kernel density (BKD) between the reference simulation (Ref.) and the scenario that employs the mean vertical N_{d} profile (S4). For the CREs, BKD are presented for the SW radiation at the TOA (a) and BOA (c), and for the LW radiation at the TOA (b) and BOA (d). The corresponding Pearson (Pears.) correlations are highlighted.

List of Tables

Table R1: Mean CRE ($\mathrm{W\,m^{-2}}$) for the SW radiation. Results are given as differences between the new scenario minus the reference simulation (Δ). The root mean square error (RMSE) in $\mathrm{W\,m^{-2}}$ and the Pearson (Pears.) correlation between the new scenarios and the reference simulation are also given.

Scen.	$\mathrm{CRE_{SW,B}}$			$\mathrm{CRE_{SW,T}}$		
	Δ	RMSE	Pears.	Δ	RMSE	Pears.
S1a	−39.2	46.4	0.960	−40.1	47.0	0.952
S1b	−7.04	11.7	0.995	−6.53	11.7	0.994
S1c	−2.59	23.4	0.964	−1.86	24.3	0.951
S1d	−6.57	17.6	0.982	−5.99	18.0	0.977
S2a	−26.1	39.2	0.943	−27.1	39.8	0.930
S2b	7.74	14.2	0.991	8.19	13.6	0.990
S2c	12.9	32.4	0.943	13.7	33.6	0.921
S2d	8.53	22.6	0.971	9.10	22.9	0.964
S3a	−31.1	41.4	0.950	−32.9	42.9	0.937
S3b	1.47	10.6	0.993	1.17	10.0	0.992
S3c	6.59	27.7	0.953	6.55	29.0	0.934
S3d	2.29	19.1	0.976	2.09	19.5	0.969
S4a	−28.7	40.1	0.947	−30.3	41.4	0.934
S4b	4.97	11.7	0.993	4.80	11.1	0.992
S4c	10.1	29.9	0.949	10.2	31.2	0.928
S4d	5.72	20.4	0.975	5.67	20.8	0.967

Table R2: Mean CRE ($\mathrm{W\,m^{-2}}$) for the LW radiation. Results are given as differences between the new scenario minus the reference simulation (Δ). The root mean square error (RMSE) in $\mathrm{W\,m^{-2}}$ and the Pearson (Pears.) correlation between the new scenarios and the reference simulation are also given.

Scen.	$\mathrm{CRE_{LW,B}}$			$\mathrm{CRE_{LW,T}}$		
	Δ	RMSE	Pears.	Δ	RMSE	Pears.
S1a	−0.11	0.48	0.999	−0.04	0.19	1.000
S1b	−0.05	0.40	0.999	−0.03	0.18	1.000
S1c	−0.01	0.50	0.999	−0.01	0.22	1.000
S1d	−0.04	0.45	0.999	−0.02	0.21	1.000
S2a	0.40	0.79	0.998	0.23	0.51	0.999
S2b	0.51	0.82	0.998	0.27	0.53	0.999
S2c	0.55	0.85	0.998	0.29	0.54	0.999
S2d	0.52	0.83	0.998	0.28	0.53	0.999
S3a	−0.05	0.74	0.997	0.33	0.64	0.999
S3b	−0.01	0.73	0.997	0.36	0.65	0.999
S3c	0.02	0.83	0.996	0.37	0.68	0.998
S3d	0.00	0.75	0.997	0.37	0.65	0.999
S4a	0.11	0.71	0.997	0.31	0.59	0.999
S4b	0.21	0.70	0.998	0.34	0.60	0.999
S4c	0.24	0.76	0.997	0.37	0.62	0.999
S4d	0.22	0.72	0.997	0.35	0.61	0.999

Table R3: Correlations between the cloud radiative effects and the cloud properties for the two major clusters characterized by low N_{int} values (L) and high N_{int} values (H). For the SW (LW) radiation, results are presented in case of the Spearman (Pearson) correlation.

Properties	$\mathrm{CRE_{SW,B}}$		$\mathrm{CRE_{SW,T}}$		$\mathrm{CRE_{LW,B}}$		$\mathrm{CRE_{LW,T}}$	
	L	H	L	H	L	H	L	H
Q_{L}	−0.935	−0.988	−0.930	−0.978	−0.016	−0.309	0.216	0.303
τ	−0.992	−0.994	−0.983	−0.986	0.028	−0.324	0.195	0.291
N_{int}	−0.446	−0.128	−0.410	−0.105	0.419	0.202	-0.259	−0.067
r_{int}	−0.343	−0.867	−0.353	−0.854	−0.311	−0.365	0.323	0.268
CBH	0.143	−0.213	−0.057	−0.292	−0.311	−0.239	0.752	0.786
CTH	−0.122	−0.604	−0.201	−0.663	−0.302	−0.376	0.783	0.717
H	−0.776	−0.921	−0.787	−0.925	−0.024	−0.386	0.217	0.300
f_{ad}	−0.126	−0.271	−0.129	−0.256	−0.003	0.144	0.215	0.194

Table R4: Explained variance and cumulative explained variance from different components obtained by the rotational component analysis (RC).

	RC-1	RC-2	RC-3	RC-4	RC-5	RC-6	RC-7	RC-8	RC-9
Explained variance (%)	33.8	35.5	14.8	13.6	2.10	0.10	0.10	0.00	0.00
Cumulative proportion (%)	33.8	69.3	84.1	97.7	99.8	99.9	100	100	100

Table R5: Pearson correlations between the logarithm of the cloud properties and the rotational components (RC). Degree of correlation (absolute values): (a) very weak: below 0.2, (b) weak: [0.2, 0.4), (c) moderate: [0.4, 0.6), (d) strong: [0.6, 0.8), and (e) very strong [0.8, 1.0].

Properties	RC-1	RC-2	RC-3	RC-4
CBH	0.969	0.025	−0.001	0.201
CTH	0.919	−0.282	0.076	0.237
Γ_{ad}	−0.896	−0.014	0.073	−0.183
τ	−0.062	−0.971	−0.192	−0.125
Q_{L}	0.036	−0.968	−0.240	0.052
H	0.177	−0.937	0.285	0.094
f_{ad}	−0.010	−0.099	−0.995	−0.025
N_{int}	−0.518	−0.250	−0.244	−0.778
r_{int}	0.382	−0.536	−0.314	0.681

Table R6: Input parameters for the RRTMG model.

Parameter	Value
Cosine of solar zenith angle	0.70
Carbon dioxide concentration	399 ppm
Ultraviolet/Visible surface albedo for direct radiation	0.05
Ultraviolet/Visible surface albedo for diffuse radiation	0.05
Near-infrared surface albedo for direct radiation	0.30
Near-infrared surface albedo for diffuse radiation	0.30

Table R7: Simulated scenarios. For scenarios S1–S3, three individual simulations (sub-cases) have been conducted according to different values for the droplet number concentration.

Scenarios	
Ref.	Double–moment scheme
S1	Single–moment scheme
S2	Vertical homogeneous model
S3	Sub–adiabatic model
S4	Mean vertical N_{d} profile
Sub-cases	a. 220 cm^{-3} b. N_{int} c. 480 cm^{-3}

Table R8: Mean and standard deviation of modeled CREs ($\mathrm{W\,m}^{-2}$) for the SW, LW, and NET (SW + LW) radiation for the reference simulation over all case days. ATM stands for the atmospheric cloud radiative effect defined as the difference between the CREs at the TOA and BOA.

Ref.	$\mathrm{CRE}_{\mathrm{SW}}$	$\mathrm{CRE}_{\mathrm{LW}}$	$\mathrm{CRE}_{\mathrm{NET}}$
TOA	-348.7 ± 78.39	17.51 ± 10.04	-331.2 ± 77.27
ATM	32.94 ± 12.11	-39.16 ± 13.14	-6.225 ± 12.98
BOA	-381.6 ± 86.95	56.66 ± 9.746	-324.9 ± 86.51

Table R9: Mean CRE ($\mathrm{W\,m^{-2}}$) for the SW radiation. Results are given as differences between the new scenario minus the reference simulation (Δ). The root mean square error (RMSE) in $\mathrm{W\,m^{-2}}$ and the Pearson (Pears.) correlation between the new scenarios and the reference simulation are also given.

Scen.	$\mathrm{CRE_{SW,B}}$			$\mathrm{CRE_{SW,T}}$		
	Δ	RMSE	Pears.	Δ	RMSE	Pears.
S1a	−39.2	46.4	0.960	−40.1	47.0	0.952
S1b	−7.04	11.7	0.995	−6.53	11.7	0.994
S1c	−2.59	23.4	0.964	−1.86	24.3	0.951
S2a	−26.1	39.2	0.943	−27.1	39.8	0.930
S2b	7.74	14.2	0.991	8.19	13.6	0.990
S2c	12.9	32.4	0.943	13.7	33.6	0.921
S3a	−31.1	41.4	0.950	−32.9	42.9	0.937
S3b	1.47	10.6	0.993	1.17	10.0	0.992
S3c	6.59	27.7	0.953	6.55	29.0	0.934
S4	−3.13	16.7	0.983	−3.16	17.2	0.977

Table R10: Correlations between the cloud radiative effects for the reference simulation (Ref.) and the cloud properties. For the SW (LW) radiation, results are presented in case of the Spearman (Pearson) correlation.

Properties	$\mathrm{CRE_{SW,B}}$	$\mathrm{CRE_{SW,T}}$	$\mathrm{CRE_{LW,B}}$	$\mathrm{CRE_{LW,T}}$
	Spearman		Pearson	
Q_L	−0.957	−0.955	−0.129	0.181
τ	−0.994	−0.987	0.104	0.148
N_int	−0.471	−0.431	0.428	−0.290
r_int	−0.446	−0.460	−0.395	0.344
CBH	0.148	0.063	−0.389	0.752
CTH	0.143	−0.220	−0.428	0.765
H	−0.795	−0.812	−0.200	0.226
f_ad	−0.284	−0.273	0.145	0.134

Table R11: Mean CRE ($\mathrm{W\,m^{-2}}$) for the LW radiation. Results are given as differences between the new scenario minus the reference simulation (Δ). The root mean square error (RMSE) in $\mathrm{W\,m^{-2}}$ and the Pearson (Pears.) correlation between the new scenarios and the reference simulation are also given.

Scen.	$\mathrm{CRE_{LW,B}}$			$\mathrm{CRE_{LW,T}}$		
	Δ	RMSE	Pears.	Δ	RMSE	Pears.
S1a	−0.11	0.48	0.999	−0.04	0.19	1.000
S1b	−0.05	0.40	0.999	−0.03	0.18	1.000
S1c	−0.01	0.50	0.999	−0.01	0.22	1.000
S2a	0.40	0.79	0.998	0.23	0.51	0.999
S2b	0.51	0.82	0.998	0.27	0.53	0.999
S2c	0.55	0.85	0.998	0.29	0.54	0.999
S3a	−0.05	0.74	0.997	0.33	0.64	0.999
S3b	−0.01	0.73	0.997	0.36	0.65	0.999
S3c	0.02	0.83	0.996	0.37	0.68	0.998
S4	−0.02	0.49	0.999	−0.02	0.22	1.000

References

[1] R. Heinze, A. Dipankar, C. C. Henken, C. Moseley, O. Sourdeval, S. Trömel, X. Xie, P. Adamidis, F. Ament, H. Baars, C. Barthlott, A. Behrendt, U. Blahak, S. Bley, S. Brdar, M. Brueck, S. Crewell, H. Deneke, P. Di Girolamo, R. Evaristo, J. Fischer, C. Frank, P. Friederichs, T. Göcke, K. Gorges, L. Hande, M. Hanke, A. Hansen, H.-C. Hege, C. Hoose, T. Jahns, N. Kalthoff, D. Klocke, S. Kneifel, P. Knippertz, A. Kuhn, T. van Laar, A. Macke, V. Maurer, B. Mayer, C. I. Meyer, S. K. Muppa, R. A. J. Neggers, E. Orlandi, F. Pantillon, B. Pospichal, N. Röber, L. Scheck, A. Seifert, P. Seifert, F. Senf, P. Siligam, C. Simmer, S. Steinke, B. Stevens, K. Wapler, M. Weniger, V. Wulfmeyer, G. Zängl, D. Zhang, and J. Quaas, "Large-eddy simulations over germany using icon: a comprehensive evaluation," *Q. J. R. Meteorol. Soc.*, vol. 143, no. 702, pp. 69–100, 2017.

[2] A. Gassmann and H.-J. Herzog, "Towards a consistent numerical compressible non-hydrostatic model using generalized hamiltonian tools," *Q. J. Roy. Meteor. Soc.*, vol. 134, no. 635, pp. 1597–1613, 2008.

[3] A. Dipankar, B. Stevens, R. Heinze, C. Moseley, G. Zängl, M. Giorgetta, and S. Brdar, "Large eddy simulation using the general circulation model icon," *J. Adv. Model. Earth Syst.*, vol. 7, no. 3, pp. 963–986, 2015.

[4] H. Wan, M. A. Giorgetta, G. Zängl, M. Restelli, D. Majewski, L. Bonaventura, K. Fröhlich, D. Reinert, P. Rípodas, L. Kornblueh, and J. Förstner, "The icon-1.2 hydrostatic atmospheric dynamical core on triangular grids – part 1: Formulation and performance of the baseline version," *Geosci. Model Dev.*, vol. 6, no. 3, pp. 735–763, 2013.

[5] A. Seifert and K. D. Beheng, "A two-moment cloud microphysics parameterization for mixed-phase clouds. part 1: Model description," *Meteorol. Atmos. Phys.*, vol. 92, no. 1, pp. 45–66, 2006.

[6] L. B. Hande, C. Engler, C. Hoose, and I. Tegen, "Parameterizing cloud condensation nuclei concentrations during hope," *Atmos. Chem. Phys.*, vol. 16, no. 18, pp. 12059–12079, 2016.

[7] A. Macke, P. Seifert, H. Baars, C. Barthlott, C. Beekmans, A. Behrendt, B. Bohn, M. Brueck, J. Bühl, S. Crewell, T. Damian, H. Deneke, S. Düsing, A. Foth, P. Di Girolamo, E. Hammann, R. Heinze, A. Hirsikko, J. Kalisch, N. Kalthoff, S. Kinne, M. Kohler, U. Löhnert, B. L. Madhavan, V. Maurer, S. K. Muppa, J. Schween, I. Serikov, H. Siebert, C. Simmer, F. Späth, S. Steinke, K. Träumner, S. Trömel, B. Wehner, A. Wieser, V. Wulfmeyer, and X. Xie, "The hd(cp)^2 observational prototype experiment (hope) – an overview," *Atmos. Chem. Phys.*, vol. 17, no. 7, pp. 4887–4914, 2017.

[8] M. Lebsock and H. Su, "Application of active spaceborne remote sensing for understanding biases between passive cloud water path retrievals," *J. Geophys. Res.-Atmos.*, vol. 119, no. 14, pp. 8962–8979, 2014.

[9] R. Wood and D. L. Hartmann, "Spatial variability of liquid water path in marine low cloud: The importance of mesoscale cellular convection," *J. Climate*, vol. 19, no. 9, pp. 1748–1764, 2006.

[10] R. Wood, "Relationships between optical depth, liquid water path, droplet concentration, and effective radius in adiabatic layer cloud," *University of Washington*, vol. 3, 2006.

[11] J. Quaas, O. Boucher, and U. Lohmann, "Constraining the total aerosol indirect effect in the lmdz and echam4 gcms using modis satellite data," *Atmos. Chem. Phys.*, vol. 6, no. 4, pp. 947–955, 2006.

[12] D. P. Grosvenor, O. Sourdeval, P. Zuidema, A. Ackerman, M. D. Alexandrov, R. Bennartz, R. Boers, B. Cairns, J. C. Chiu, M. Christensen, H. Deneke, M. Diamond, G. Feingold, A. Fridlind, A. Hünerbein, C. Knist, P. Kollias, A. Marshak, D. McCoy, D. Merk, D. Painemal, J. Rausch, D. Rosenfeld, H. Russchenberg, P. Seifert, K. Sinclair, P. Stier, B. van Diedenhoven, M. Wendisch, F. Werner, R. Wood, Z. Zhang, and J. Quaas, "Remote sensing of droplet number concentration in warm clouds: A review of the current state of knowledge and perspectives," *Rev. Geophys.*, vol. 56, no. 2, pp. 409–453, 2018.